JCRS

Journal of Chemical Reactivity and Synthesis 2023: 13(4) 321-350

Research Article

Ultrasound- and Magnetic Assisted Dispersive-Micro-Solid-Phase Extraction followed by Atomic Absorption Spectrometry based on Carbon Quantum Dots Functionalized with Magnetite/Zeolitic Imidazolate Framework 71/Polypyrrole for Determination and Trace Monitoring of Pb (II) in Water and Food Samples

Elnaz Nakhostin Mortazavi, Mohsen Zeeb*, Seyed Saied Homami

Department of Applied Chemistry, Faculty of Science, South Tehran Branch, Islamic Azad University, Tehran, Iran.

ARTICLE INFO:

Received:
16 April 2024

Accepted:
13 June 2024

Available online:
15 June 2024

✉: M. Zeeb
zeeb.mohsen@gmail.com

ABSTRACT

A new method called ultrasound-& magnetic-assisted dispersive micro-solid-phase extraction (US-M-A-DMSPE) was developed for the selective separation of lead ion using an innovative nanocomposite based on carbon quantum dots functionalized with magnetite/zeolitic imidazolate framework 71/polypyrrole. The Pb (II) ion was analyzed by flame atomic absorption spectrometry (FAAS). The nanosorbent's structure was characterized using scanning electron microscopy (SEM), transmission electron microscopy (TEM), X-ray diffraction (XRD), energy-dispersive X-ray analyzer (EDX), vibrating sample magnetometry (VSM), and Fourier transform-infrared (FT-IR) spectroscopy. Optimum experimental conditions and analytical parameters, such as the amount of sorbent, sample pH, ultrasonic time, chelating agent concentration, ionic strength, volume of desorbing solvent and reusability were determined to achieve maximum recoveries of Pb (II). Under the optimal conditions, the preconcentration factor was achieved 60. The limits of detection and quantification were found to be 0.15 ng mL^{-1} and 0.5 ng mL^{-1}, respectively.

Keywords: Lead; Carbon quantum dot; Fe_3O_4; ZIF-71; Polypyrrole; Flame atomic absorption spectrometry.

1. Introduction

The presence of heavy metal contamination can be attributed to both natural and industrial sources, which are persistent in the environment and have the ability to accumulate in living organisms. This poses a major threat to both human health and the environment. Lead, a highly toxic and non-biodegradable element, is particularly harmful and can cause serious health issues, such as anemia, cardiovascular problems, developmental disorders, and damage to various bodily systems, including the liver, kidneys, endocrine, hematopoietic, and reproductive systems [1-2]. The International Agency for Research on Cancer (IARC) has classified lead as a human carcinogen. Due to its widespread and hazardous nature, it is crucial to monitor and measure lead levels in food and water samples [3]. Several techniques, such as inductively coupled plasma mass spectrometry (ICP-MS) [4], inductively coupled plasma optical emission spectrometry (ICP OES) [5], electrothermal atomic absorption spectrometry (ETAAS) [6], and graphite furnace atomic absorption spectroscopy (GF-AAS) [7], have been used for lead analysis. However, these methods have limitations and can be complex, time-consuming, and involve the use of potentially hazardous reagents. Therefore, it is essential to establish a fast, simple, and sensitive method for detecting lead (II) analysis. In recent years, flame atomic absorption spectrometry (FAAS) has emerged as a promising alternative. The main objective of this study is to concentrate and purify the analyte, followed by the trace determination of lead in water and food samples [8]. Sample preparation is a crucial step in trace analytical methods, and its advantages include extraction time, solvent volume, repeatability, ease, cost, and automation [9-10]. It is important to select the appropriate sample preparation method for qualitative and quantitative determination of target compounds. Various methods have been developed in extraction for pre-concentrate and trace monitor heavy metals. liquid-liquid extraction (LLE) and solid-phase extraction (SPE) being the most commonly used techniques. However, LLE has limitations such as

being tedious, time-consuming, and expensive, whereas SPE offers several benefits, including repeatability, automation, low organic solvent consumption, high extraction capacity, high enrichment factor, simplicity, and low cost [11-12]. Nonetheless, SPE has limitations such as sorbent clogging, the requirement of toxic solvent and high column pressure [13]. Magnetic solid-phase extraction (MSPE) is an attractive and classical method, the most interesting advantage of this method is the easy and rapid separation of magnetic sorbents, which significantly reduces the sample pretreatment time. Additionally, the dispersion of the sorbent in a large sample size allows for effective sorbent recovery using an external magnetic field. MSPE has been successfully applied in various media, including food, biological, and environmental samples [14-16].

In this method, magnetic nanosorbents such as Fe_3O_4 nanoparticles with high surface-area-to-volume ratio, low toxicity, high extraction speed and high adsorption capacity improve the extraction efficiency and it also allows for easier and faster sorbent isolation from the sample media by using an external magnetic field.

Various nanomaterials have been employed in MSPE, and the type of sorbent plays a crucial role in the performance of the technique, influencing selectivity, stability, dispersibility, and extraction capability [17-19]. Therefore, the production of novel coating materials for sorbents has received significant attention.

Carbon nanomaterials have recently gained attention as sorbents due to their unique features, including facile synthesis, excellent dispersion in water, favorable biocompatibility, high sensitivity, selectivity, stability, low toxicity, and environmental friendliness. Among this materials, carbon quantum dots (CQDs), a subgroup of carbon-based nanomaterials, are obtained during the purification of single-walled carbon nanotubes through preliminary electrophoresis. With their remarkably small size (approximately 10 nm) and oxygen-containing groups on their surface (hydroxyl, epoxy, carbonyl, and carboxyl), CQDs exhibit a

high adsorption capacity and a suitable surface-to-volume ratio. These properties make them promising sorbents in separation science. Moreover, modifying their surface can alter their physical properties, such as solubility in aqueous and non-aqueous solvents. Due to their large polar moieties and dispersing capability in aqueous solutions, CQDs have been successfully utilized in the extraction process [20-23].

Magnetic carbon quantum dot nanoparticles (CQD/Fe_3O_4) represent a superior sorbent due to their combination of magnetic properties and the unique features of CQDs. In this case, CQDs are coated with magnetic nanoparticles to prevent their aggregation and enhance the adsorption capacity and extraction efficiency [24-25].

Another class of materials that has gained attention in recent years is metal-organic frameworks (MOFs). MOFs are hybrid inorganic and organic supramolecular materials based on the coordination of metal ions or clusters with bi- or multidentate organic linkers. The properties of MOFs include uniformly structured cavities and tunable pore sizes, making them suitable for hosting guest molecules. As a result, MOFs are widely used as sorbents in separation processes for various samples, including environmental samples, food samples, and drinking water [26-28]. Zeolitic imidazolate frameworks (ZIFs) are a subgroup of crystalline MOFs with extensive three-dimensional structures and zeolite-like topology. They have demonstrated excellent sorbent properties due to their large surface areas and superior hydrothermal and chemical stabilities. The combination of carbonaceous materials with ZIFs significantly enhances the sorbent's benefits and makes it a promising sorbent for sample preparation and separation purposes [29-30].

Among various ZIFs, ZIF-71 is one of the most superior materials for forming hybrid materials that are synthesis at room temperature. Also, it has a RHO topology with an eight-membered-ring size of 0.48 nm and a large cage size of 1.68 nm. ZIF-71 exhibits high sorption capacity and offers attractive features such as short preparation time, simple

synthesis route, low cost, high surface area, and low density [31-32]. Several composites of ZIF-71 have been developed, including ZIF-71/CC [33], WO_3@ZIF-71 [34], ZnO@ZIF-71 [35], and MoS_2@ZIF-71 [36]. In this study, ZIF-71 was selected as a modifier agent for CQDs due to its mentioned features that enhance the sorbent's quality and extraction efficiency. Generally, ZIFs have a greater tendency to be combined with polymers compared to traditional inorganic particles due to their structural flexibility. Among different types of coating sorbents used for the extraction of organic analytes, conductive polymers (CPs) due to their excellent chemical, mechanical and thermal stability, their ability to establish π-π interactions, their large surface area, polar functional groups and ion exchange property are used as practical sorbent.

Polypyrrole (PPy), the most common candidate in the class of CPs, can interact with analyte molecules via ion-exchange, hydrogen bonding or electrostatic interactions. Due to its unique properties such as benign nature, low manufacturing cost, easy synthesis and high surface area, PPy has gained considerable interest for SPE method for a wide variety of analytes including drugs, pesticides, and heavy metals. In addition, modification of the sorbent synthesized with PPy improves the quality of the sorbent and made better the mass transfer capacity of the sorbent material [37-39].

The objective of this work was to prepare a new type of sorbent for the preconcentration and separation of Pb (II) using ultrasound-& magnetic-assisted dispersive micro-solid-phase extraction (US-M-A DMSPE), followed by flame atomic absorption spectrometry (FAAS) analysis of food and water samples. In this developed system, the surface of CQD was magnetized with Fe_3O_4 particles, and then the fabricated sorbent surface was coated with ZIF-71 and PPy to create a promising sorbent. This proposed method offers advantages such as low cost, simplicity, safety, and a high capacity for concentrating Pb (II). The main parameters affecting the extraction performance were investigated and optimized. Ultimately,

the combination of the extraction technique with FAAS provides an analytical procedure for assessing trace levels of lead in water and food samples.

2. Experimental

In all steps, analytical grade of each chemical material was used without further purification. 4, 5-Dichloroimidazole, zinc acetate, pyrrole, ferric chloride and citric acid were obtained from Sigma-Aldrich (St. Louis, MO, USA). Iron (III) chloride hexahydrate, iron (II) chloride tetrahydrate, ethanol, methanol, chloroform, acetonitrile, urea, 25% ammonia solution, nitric acid, hydrogen peroxide, acid, hydrochloric acid, sodium hydroxide and perchloric acid were purchased from Merck Chemicals (Darmstadt, Germany). Ultrapure water was employed in all experiments (Millipore, Bedford, MA, USA).

According to standard methods [4], the standard stock solution of Pb (II) (100 mg L^{-1}) was prepared from analytical reagent grade (AR) $Pb(NO_3)_2$. Diphenylthiocarbazone (dithizone, formula weight= 256.33) was purchased from BDH Limited, Poole, England and used as received.

2.1. Instrumention

A Shimadzu AA-6300 (Kyoto, Japan) atomic absorption was used for lead measurements. Hollow-cathode lamp (Hamamatsu Photonics, Shizuoka, Japan) at wavelength of 283.3 nm and current of 10 mA with a spectral bandpass 0.7 nm was applied to determine lead. The X-ray diffraction (XRD) spectra were recorded and investigated by applying Kα radiation (λ = 1.54 Å) as the X-ray produced by Cu element via a D8 Advance X-ray diffractometer (Bruker, Germany). Fourier transform infrared (FT-IR) spectra recordings were carried out by applying Perkin Elmer FTIR spectrometer (RXI, Germany). Transmission electron microscopic (TEM) image was recorded using HT7800 (Hitachi, Japan), Scanning electron microscopy (SEM) images and energy-dispersive X-ray (EDX) spectra were recorded and examined using TESCAN-Vega 3 machine (TESCAN, Czech Republic) and Zeiss Sigma VP

machine (Jena, Germany). Magnetization measurements were performed on a vibrating sample magnetometry (VSM, MDKB, Iran).

2.2. Preparation of real sample

Water samples

To determine the amount of Pb (II) using the proposed method, different samples of mineral and tap water were utilized. Bottled mineral water was purchased from a local store, and tap water was collected from the water faucet in the lab located in Tehran, Iran. Initially, the samples were collected in polyethylene bottles that were cleaned with detergents, diluted nitric acid, and water. Then, approximately 50 mL of each water sample was filtered using a 0.45 μm Millipore filter and stored in 100 mL plastic bottles, and the preconcentration method was employed to analyze the water samples. Subsequently, the concentration of the analyte in the samples was determined using flame atomic absorption spectroscopy.

Potato and carrot

Potato and carrot samples were purchased from a marketplace in Tehran, Iran. 1 g of potato and carrot were washed with distilled water and detergent. They were then transferred to a silica crucible and dried in an oven at 120 ºC until a constant weight was achieved. The obtained samples were placed into a muffle furnace and heated to 400 ºC for 12 h to turn them into ash.

After the residue reached ambient temperature, it was treated with 10 mL of concentrated nitric acid and 3 mL of 30% (w/w) H_2O_2. Then, it was kept in an oven at 400 °C for 4 h.

Finally, the remaining sample was digested with 3 mL of concentrated hydrochloric acid and 3 mL of 70% (w/v) perchloric acid. The vapors were evaporated with heat, and the resulting solution was transferred into a volumetric flask and diluted to 1000 mL.

Milk

A fresh milk sample was obtained from a local supermarket in Damavand, Iran. 5 mL of nitric acid and 2 mL of hydrogen peroxide were added to 5 mL of fresh milk at a relatively low temperature for the digestion process to prevent mutation. After the residue reached room temperature, the solution was dissolved in 1 mL of 0.1 mol/L HNO_3 and 10 mL of distilled water. It was then filtered using a filter paper and transferred to a 50 mL volumetric flask. Finally, the volume was adjusted to 50 mL by adding distilled water. This SPE method was applied to the real sample, and the concentrations of analytes were determined by FAAS.

2.3. Synthesis of CQD

Carbon quantum dots were synthesized using the hydrothermal method from citric acid and urea as prefabrication and water as the solvent. Briefly, 3 g of citric acid was added to 1 g of urea and dissolved in 20 mL of deionized water. The solution was thoroughly mixed with a magnetic stirrer for 5 min at room temperature, resulting in a clear solution. It was then heated to 200°C in an autoclave for 6 h, leading to the formation of a foam structure. After reaching room temperature, the black powder of CQD was obtained [40].

2.4. Modifying of carbon quantum dots with Fe_3O_4 nanoparticles

Modyfing of carbon quantum dots with Fe_3O_4 nanoparticles was achieved using the co-precipitation method. Initially, 0.3 g of CQD was dispersed in 150 mL of deionized water using an ultrasonic bath for 30 min. Then, $FeCl_3.6H_2O$ (0.825g) and $FeCl_2.4H_2O$ (0.322g) were dissolved in 25 mL of deionized water. The solution of iron (II) and (III) was added dropwise to the CQD solution at room temperature (22 ± 0.5 °C) under a nitrogen atmosphere. After both salts dissolved, ammonia (25% v/v) was added until the solution reached a pH of 10. The resulting black suspension was vigorously stirred at 80 ºC for 30 min. The solution containing the synthesized CQD/Fe_3O_4 nanoparticles was then centrifuged, and the nanoparticles were dried at 100 °C in an oven after being washed several times with methanol [41].

2.5. Synthesis of CQD/Fe_3O_4/ZIF-71

In a typical procedure, 0.0743 g of zinc acetate and 0.2182 g of 4, 5-dichloroimidazole were dissolved in 15 mL of methanol, respectively, to form a clear solution, then the two solutions were combined together in a sealed vial. After that, 0.25 g CQD/ Fe_3O_4 was added into the prepared solution and placed at room temperature for a night. The next step, methanol was removed by utilizing a pipette and the formed crystals were soaked three times with 20 mL of chloroform solvent for 72 h. Lastly, the final product was obtained under vacuum at 90°C for 1 h [42].

2.6. Synthesis of CQD/Fe_3O_4/ZIF-71/PPy

Briefly, 0.2 g of CQD/ Fe_3O_4/ZIF-71 was dispersed into 50 mL of deionized water, then 0.8 mL of pyrrole (PPy) monomer was added into 25 mL of deionized water. Next step, the fresh pyrrole solution was mixed with the CQD/ Fe_3O_4/ZIF-71 solution slowly under stirring in an ice bath for 2 h. 10 g oxidizing agent ($FeCl_3 \cdot 6H_2O$) were dispersed in 25 mL of deionized water and added into this solution and followed by Polymerization was carried out for 12 h under N_2 gas flow and an ice bath.

Eventually, the product was filtered and washed several times with water and ethanol to remove the unreacted pyrrole and excess ferric chloride and dried into oven at 60 ºC [43]. Schematic representation for fabrication of CQD/ Fe_3O_4/ZIF-71/PPy nanocomposite are shown in Figure 1.

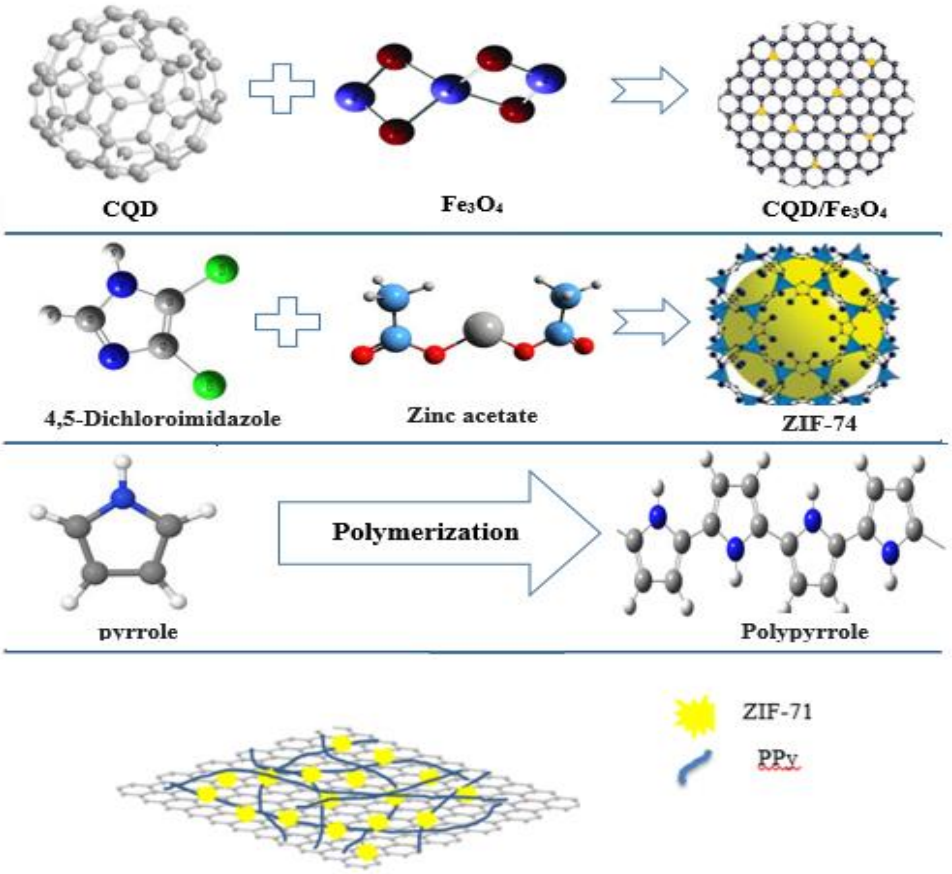

Fig. 1. Schematic representation for the fabrication of CQD/ Fe_3O_4/ZIF-71/PPy.

2.7. Ultrasound-and magnetic-assisted dispersive micro-solid-phase extraction process

A Schematic of the US-M-A-DMSPE-FAAS procedure is illustrated in Figure 2. Initial, 30 mL of the samples/standard solution was added to the glass tube, containing 50 μM Dithizone. The pH of the samples solution was adjusted to 6 with buffer. In addition, to eliminate possible interference caused by other species, an excess amount of dithizone reagent (90 μM) was used in real samples. Then, 25 mg of the magnetic sorbent were added to the sample solution containing the analyte. Subsequently, the solution was sonicated for 6 min to assist sorption of the analyte onto the surface of CQD/ Fe_3O_4/ ZIF-71/PPy sorbent. next, the magnetic sorbent was separated and collected from sample media via a strong magnet (5 cm × 5 cm × 5 cm, 0.8 Tesla) and the supernatant was directly removed. Elution

was performed with 500 µL of 50% V/V HNO_3 2M in ethanol and was subjected to ultrasound for 2 min. Eventually, the magnet was utilized once more to separate the sorbent, and desorbed analyte determined with FAAS analysis.

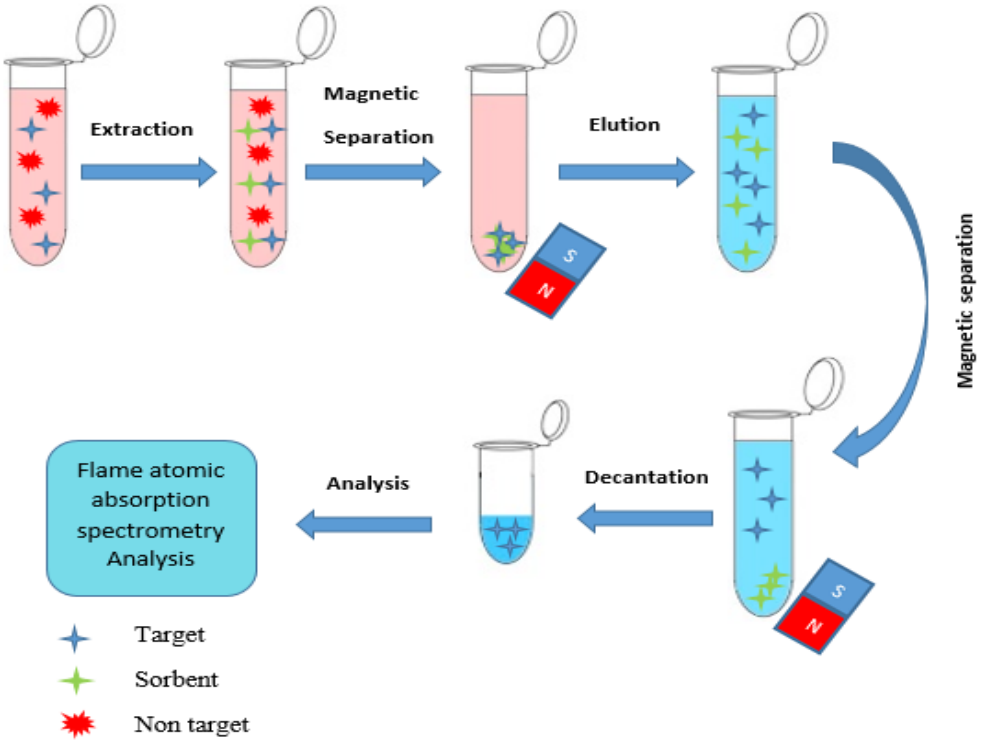

Fig. 2. Illustration of the US-M-A-DMSPE-FAAS process for determination of Pb (II).

3. Result and discussion

3.1. Characterizations

Various instrumental analytical techniques including FTIR, XRD, EDX, SEM, TEM, and VSM were employed to characterize the nanocomposite sorbent. The FTIR spectra of CQD, CQD/Fe_3O_4, CQD/Fe_3O_4/ZIF-71, and CQD/Fe_3O_4/ZIF-71/PPy (Figure 3a-d) were analyzed to confirm the structure of the nanosorbent.

In the FTIR spectrum of CQD (Figure 3a), the presence of hydroxyl group (O-H) stretching vibrations is confirmed by observing a broad peak at a wavenumber of 3100-3300

cm^{-1}. Additionally, three characteristic peaks located at 1593, 1444, and 1182 cm^{-1} are assigned to the C=O group, the aromatic C=C bond, and the stretching vibrations of epoxy C-O. Compared with the spectrums of CQD/Fe_3O_4 nanoparticles, the peak at 614.26 cm^{-1} can be related to stretching vibrations of Fe-O in the magnetic nanoparticles (Fig 3b). Moreover, the presence of a broad band at 3327 cm^{-1} and an intense band at 1613 cm^{-1} indicates -OH stretching vibrations on the surface of Fe_3O_4 nanoparticles [44]. In the spectrum of CQD/Fe_3O_4/ZIF-71 (Figure 3c), most of the absorption bands are assigned the stretching of imidazole units, for instance, the peak at 1461 cm^{-1} is associated with the C=N stretch mode, while the strong bands at 1198 cm^{-1} are attributed to the C-N stretching of the imidazole units. The spectral regions of 900-1350 cm^{-1} are assigned to in-plane bending, and those below 800 cm^{-1} are related to the out-of-plane bending of the imidazole ring [45]. Furthermore, the peak at 1523 cm^{-1} is assigned to secondary amine N-H bonds, and the peak at 3400-3500 cm^{-1} can be attributed to free non-hydrogen bonded N-H. The spectrum of ZIF-71 aligns well with the published literature, confirming successful synthesis of ZIF-71 on the CQD surface.The spectrum of CQD/Fe_3O_4/ZIF-71/PPy (Figure 3d) exhibits peaks at 1298 cm^{-1}, 961.21 cm^{-1}, and 1703 cm^{-1}, which are assigned to C-N of the pyrrole, C=C in-plane bending vibration in the pyrrole ring, and C=O stretching vibration, respectively [46-47]. These peaks confirm the action and reaction between CQD and pyrrole rings in the polymer via π-π interactions and hydrogen bonding. It can be concluded that the polymerization of PPy on the CQD/Fe_3O_4/ZIF-71 surface has been successfully achieved.

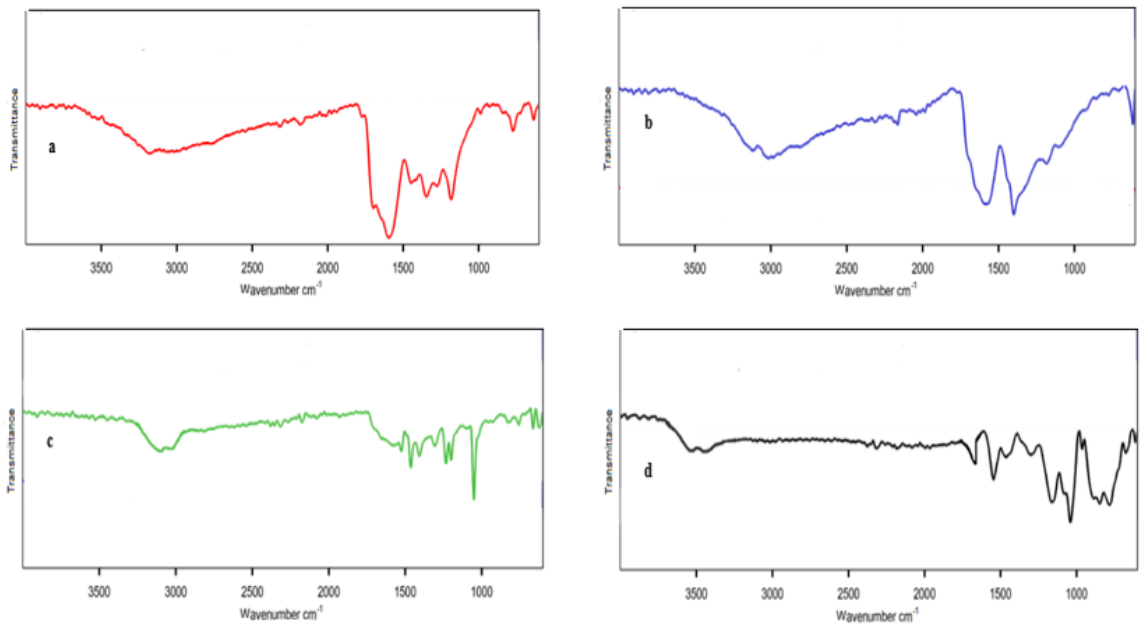

Fig. 3. Fourier transform infrared spectra of (a) CQD, (b) CQD/Fe_3O_4, (c) CQD/Fe_3O_4/ZIF-71, and (d) CQD/Fe_3O_4/ZIF-71/PPy nonporous composite.

Energy-dispersive X-ray spectroscopy (EDX) was utilized to assess the elemental composition and confirm the successful modification of the nanoscale sorbent. The EDX analysis in Figure 4 clearly demonstrates the presence of elements such as nitrogen, sulfur, iron, oxygen, zinc, and carbon in the CQD/Fe_3O_4/ZIF-71/PPy sorbent. These results validate the expected distribution of elements in the sample.

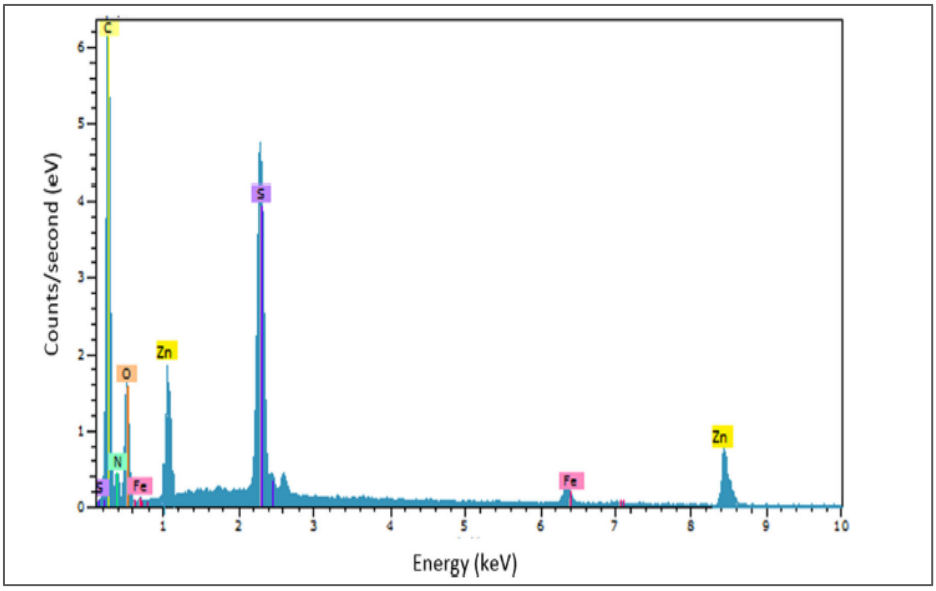

Fig. 4. Energy-dispersive x-ray spectrum of CQD/Fe_3O_4/ZIF-71/PPy.

The morphology and particle size of the CQD, CQD/Fe_3O_4, CQD/Fe_3O_4/ZIF-71, and CQD/Fe_3O_4/ZIF-71/PPy nanoporous composites were investigated using TEM and SEM micrographs. The transmission electron microscopy (TEM) image (Figure 5a) and scanning electron microscopy (SEM) image (Figure 5b) of the CQD nanosheets reveal a layered morphology with dispersed spherical particles of mean diameter below 9 nm. The images also show the presence of numerous residues, including hydroxyl and carboxyl groups on the CQD surface [48-49]. The SEM image of CQD/Fe_3O_4 (Figure 5c) confirms the formation of carbon shells around the Fe_3O_4 nanoparticles and the presence of sphere-like morphologies with a significant distribution on the CQD surface [50]. The complete dispersion of ZIF-71 crystal form is evident in Figure 5d, indicating successful surface modification of CQD/Fe_3O_4 with ZIF-71. It can be seen that the surface of CQD/ Fe_3O_4 /ZIF-71 became rougher after adding 4,5-dichloroimidazole to the solution to react with Zn^{2+} adsorbed on CQD/ Fe_3O_4 spheres, and ZIF-71 shells on CQD / Fe_3O_4 is formed [51]. The coating of conductive polymer is shown in Fig 5e, as seen in CQD/ Fe_3O_4/ZIF-71/PPy nanocomposite, PPy is well dispersed by provided a well-established plate form to CQD/ Fe_3O_4/ZIF-71 and can increase the surface area and improve the sorbent properties. The PPy may possibly avoid the agglomeration of the CQD/ Fe_3O_4/ZIF-71 due to the surface functionalities and also, it can be observed that the morphology of CQD/Fe_3O_4/ZIF-71/PPy is not significantly different from CQD/ Fe_3O_4/ZIF-71 [52-53].

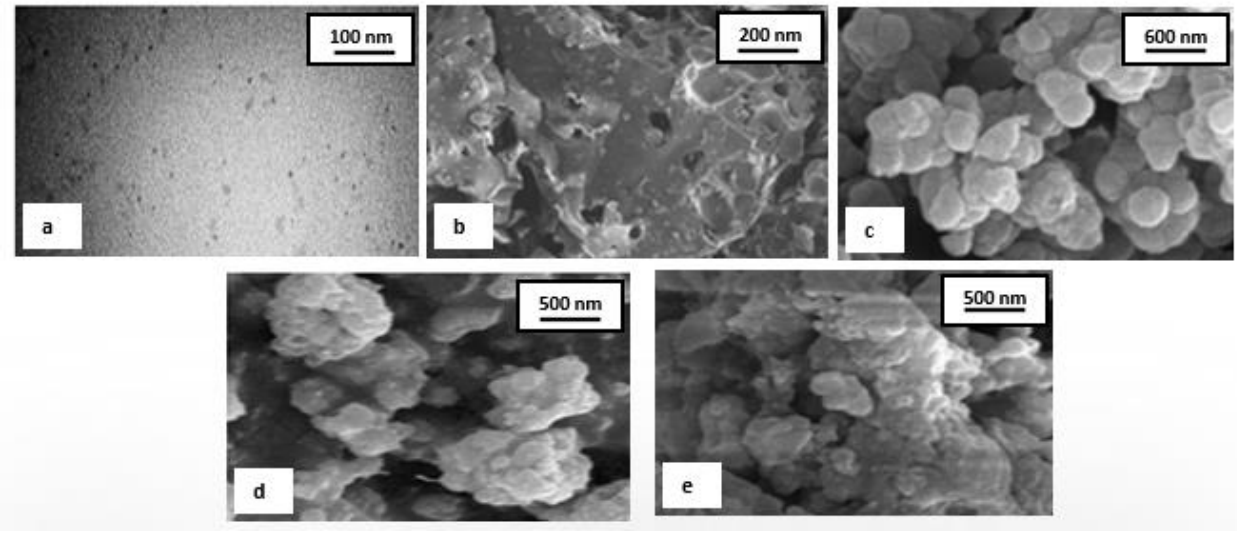

Fig. 5. Transmission electron microscopy image of (a) CQDs. Scanning electron microscope images of (b) CQDs, (c) CQD/Fe_3O_4, (d) CQD/Fe_3O_4/ZIF-71, and (e) CQD/Fe_3O_4/ZIF-71/PPy**.**

The crystal structure of the synthesized materials (CQDs, CQD/Fe_3O_4, CQD/Fe_3O_4/ZIF-71, and CQD/Fe_3O_4/ZIF-71/PPy) was examined using X-ray diffraction (XRD). The XRD patterns in Figure 6 reveal the characteristics of the synthesized nanocomposites. The XRD analysis of the prepared CQDs (Figure 6a) shows a broad peak at 2θ equal to 25°, indicating the amorphous nature of the carbonaceous material [54]. The XRD pattern of CQD/Fe_3O_4 nanocomposite (Figure 6b) exhibits peaks at 2θ = 32° (220); 35° (331); 41° (400); 54° (422); 57 ° (511); 63.4° (440), confirming the formation of Fe_3O_4, which matches the standard Fe_3O_4 XRD pattern [55]. The XRD analysis of CQD/Fe_3O_4/ZIF-71 is similar to CQD/Fe_3O_4, with the addition of a weak peak at 2θ = 7° (011), indicating the crystalline structure of ZIF-71 [56]. Figure 6d demonstrates the XRD diffraction pattern of the CQD/Fe_3O_4/ZIF-71/PPy nanocomposite, which exhibits a characteristic wide peak between 2θ = 20-30°, corresponding to the amorphous nature of PPy [57].

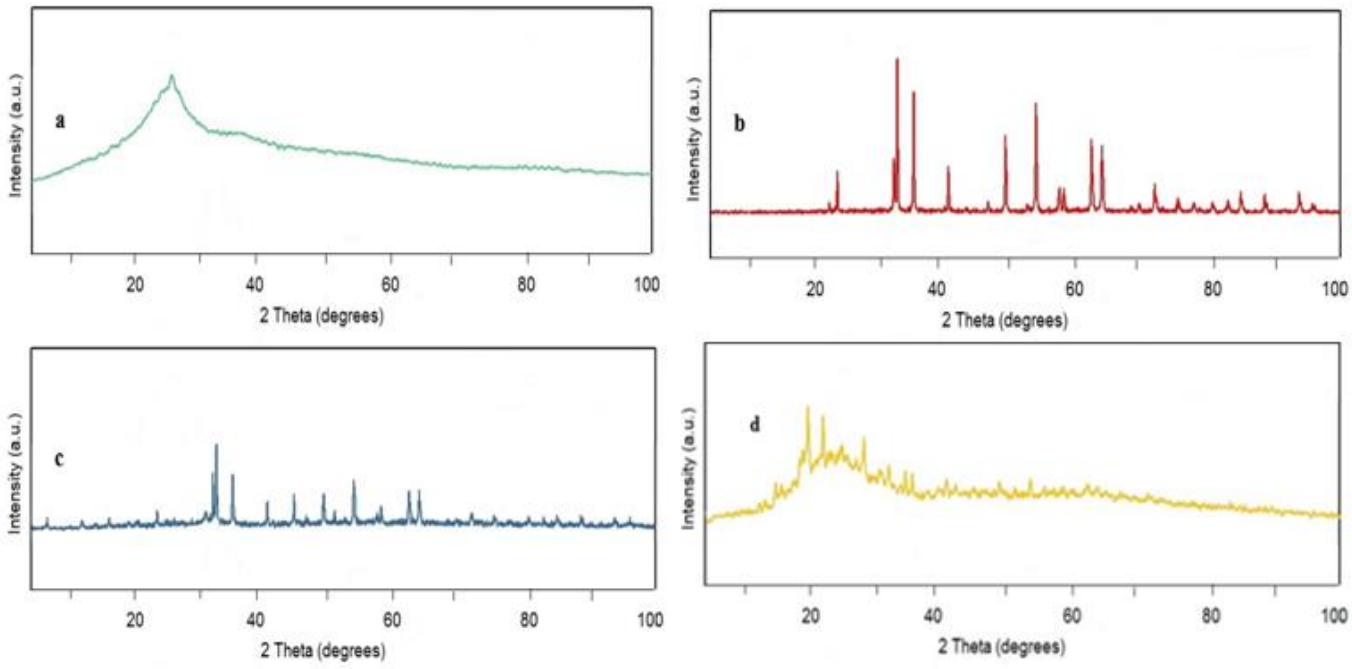

Fig. 6. X-ray diffraction patterns of CQD, CQD/Fe_3O_4, CQD/Fe_3O_4/ZIF-71, and CQD/Fe_3O_4/ZIF-71/PPy.

The VSM explains the magnetic features of a nanocomposite, also described the size and shape of the magnetization. In this study, VSM was employed to determine the magnetic saturation of the synthesized magnetic nanoparticles. Figure 7 illustrates the saturation magnetization values of Fe_3O_4, CQD/Fe_3O_4, CQD/Fe_3O_4/ZIF-71, and CQD/Fe_3O_4/ZIF-71/PPy, which are 65.3, 54.4, 38.7, and 28.9 emu g^{-1}, respectively. It can be observed that the saturation magnetization of CQD/Fe_3O_4/ZIF-71/PPy is lower than that of CQD/Fe_3O_4, indicating an increased coating amount due to the presence of PPy and ZIF-71. Though the saturation magnetization of the synthesized nanocomposite is low, it is large enough that the nanocomposite can be conveniently separated from the reaction media [58-59]. These results confirm the successful synthesis of the nanocomposite.

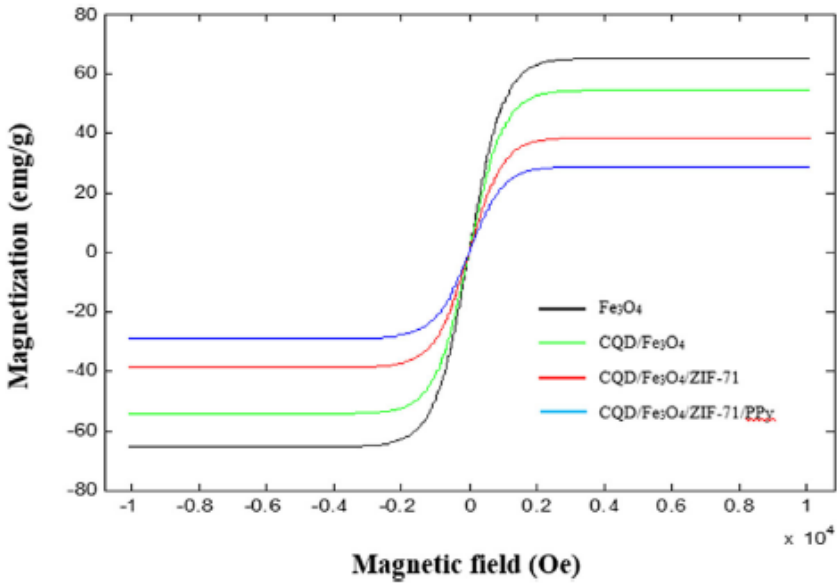

Fig. 7. Magnetization hysteresis of Fe_3O_4, CQD/Fe_3O_4, CQD/Fe_3O_4/ZIF-71, and CQD/Fe_3O_4/ZIF-71/PPy.

3.2. Optimization

In the optimization process, various parameters were investigated and optimized to enhance the extraction efficiency of the proposed method. These parameters include the amount of sorbent, pH of samples, ultrasonic time, chelating agent concentration, ionic strength, volume of desorbing solvent, and reusability of the sorbent.

3.3. Effect of sorbent amount

The amount of sorbent in extraction processes is closely related to the amount of target analyte [11]. The effect of sorbent amount was evaluated by varying the amount from 2 to 50 mg. Figure 8 shows that the peak area increased with the increasing amount of CQD/Fe_3O_4/ZIF-71/PPy until reaching the highest signal at 25 mg of sorbent and then, by adding more than 25 mg of sorbent, the extraction efficiency reduced little by little and it remained almost constant. The decrease in extraction efficiency after the maximum value may be due to less complete desorption. Therefore, the optimal amount of sorbent for achieving the best extraction efficiency was determined to be 25 mg.

3.4. Effect of chelating agent concentration

Dithizone is a hydrophobic complex that is very stable and selective and can affect the extraction efficiency [60]. Therefore, as a useful complexing agent has been chosen to extraction of lead ion in this effort. During the optimization, the effect of dithizone concentrations in the range of 5-70 µM on the absorption signals was investigated. As shown in Figure 8, the signals increased notably with increasing dithizone concentration, demonstrating that appropriate amount of complexing agent had a beneficent effect on the extraction efficiency and in higher concentrations, it has not had a significant impact on the SPE process and the analytical signals remain almost constant. Hence, 50 µM of dithizone concentration was used as the optimal value for further experiments.

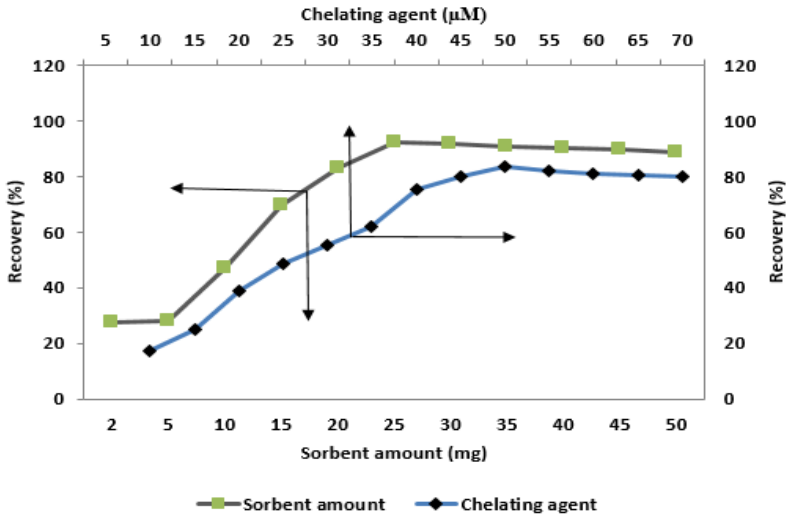

Fig. 8. Effect of CQD/Fe_3O_4/ZIF-71/PPy amount and chelating agent (dithizone) dosage on extraction recovery.

3.5. Effect of sample pH

The pH of the sample solution is a crucial factor in the US-M-A-DMSPE process. pH directly influences the reaction between the metal ion and the complexing agent, and subsequently affects the extraction efficiency of the sorbent for the target [61]. To optimize the pH, acidity was studied within a pH range of 2-12. HCl and NaOH were used to adjust the pH of the sample solution. As shown in Figure 9, with increase pH, the absorption signal also

increases, reaching its maximum value in the pH range of 6-8. However, as the pH continues to increase, the signals begin to decrease. Therefore, the optimal pH for the sample solution was selected as 6.

3.6. Effect of ultrasonic time

In the established US-M-A-DMSPE process, the degree of dispersion of the fabricated nanosorbent in the solution is directly related to the efficiency of adsorption and extraction. Ultrasonic treatment creates a turbulent state in the solution, increasing the contact surface area between the phases. This phenomenon improves the mass transfer of analytes and plays an important role in enhancing adsorption efficiency [62]. In this experiment, the ultrasonic time (extraction time) was evaluated in the range of 0-12 min. The results shown in Figure 9 demonstrate that the absorbance signal significantly increased with the assistance of ultrasound. As the ultrasonic time increased, the absorption increased up to 6 min, after which the signals slightly decreased. Therefore, the optimal ultrasonic time for extraction was determined to be 6 min. Initially, there are unfilled surface sites, but once equilibrium is reached, the remaining binding sites are hardly filled. This can be attributed to the repulsive forces between the heavy metal ions on the magnetic adsorbent and the sample solution.

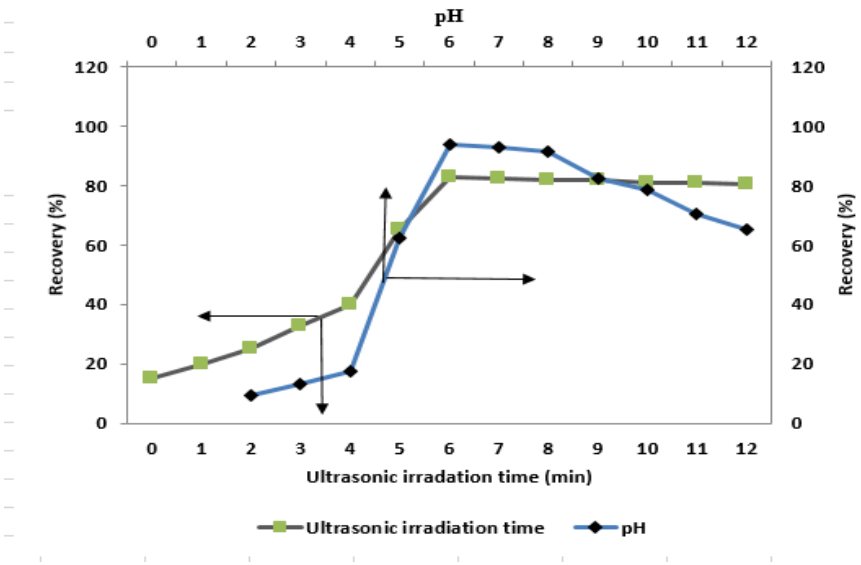

Fig. 9. Effect ultrasonication time and pH on extraction recovery.

3.7. Effect of ionic strength

The addition of salt can have several effects on the extraction efficiency. Among these effects, it can accelerate the mass transfer of the analyte to the sorbent and improve the extraction efficiency [63]. The influence of the ionic strength of the sample solution on the US-M-A-DMSPE process was investigated in the range of 0-10% w/v NaCl concentration. The results indicate that the extraction efficiency of Pb (II) increased up to 1% of NaCl concentration, after which it exhibited a constant decrease. This decrease is due to the inhibition of active sites on the sorbent by the salt ions. Therefore, 1% w/v of salt was considered as the optimal value.

3.8. Effect of desorption conditions

The choice of desorption solvent is critical for achieving high extraction efficiency. The type and volume of the desorption solvent play an important role in eluting the analytes. Analytes have different solubilities in solvents with varying polarities. Initially, methanol, ethanol, and acetonitrile were studied as desorption solvents for the quantitative recovery of Pb (II) by adding 50% v/v HNO_3 2M. The results clearly indicate that ethanol provided the best performance for the desorption of analytes. Therefore, ethanol was chosen as the optimal solvent for elution.

3.9. Reusability of the magnetic sorbent

The reusability of the magnetic nanosorbent is a main parameter that needs to be evaluated to determine the useful life of the sorbent. In this method, after the extraction, the sorbent was washed with 3 mL of ethanol and 3 mL of double-distilled water. After drying the sorbent at room temperature, it was subjected to the extraction protocol again. Under optimized conditions, six repeated adsorption/desorption cycles were performed. The evaluation of the percentage of recovery of the analytical signal (91%) indicated that after six cycles, there was

no significant loss in the sorption capacity. This demonstrates the good performance of the synthesized nanosorbent for the quantification of Pb (II) metal ions.

3.10. Effect of interference ions

Dithizone can form complexes with many metal ions, and as a result, other metal ions present may competitively form complexes with dithizone compared to lead. These complexes can affect the extraction efficiency. To evaluate the performance, reliability, and selectivity of the applied US-M-A-DMSPE method, the effect of different potential interfering ions commonly found in environmental water and food samples on the extraction efficiency and measurement of Pb (II) was investigated. For this purpose, Standard solutions containing a fixed concentration of Pb (II) (10 ng mL^{-1}) and various concentrations of interfering ions were prepared under optimal conditions. Atomic absorption was subsequently evaluated, and recovery was calculated. The results are shown in Table 1 (the tolerable limit was set as a relative error ≤ 5%). To eliminate interfering ions from real samples, 90 μM dithizone was used as an excess.

Table 1. Interference study of the interfering ions on the determination of 10 ng mL^{-1} lead using US-M-A-DMSPE –FAAS.

Interfering ions	Tolerance Ratio [Interference-to-Pb (II) ratio[a]]
K^+, Na^+, Li^+, Cl^-,$Au3^+$	1000
SO_4^{-2}, Mg^{2+},$Al3^+$	800
Ca^{2+}, NO_3^-	500
F^-, Cr^{3+},I^-	100
Mn^{2+}, Ni^{2+},Zn^{2+},Cd^{2+}	75
Fe^{3+}, Cu^{2+}, PO_4^{-3}, CO_3^{-2}	25

[a] Tolerance limit was defined as the largest ratio causing a relative error less than 5% in concentration level of lead.

3.11. Analytical performance data

Under optimal conditions, the performance of the proposed US-M-A-DMSPE-FAAS technique was assessed based on vital parameters such as calibration curves, limits of

detection (LOD), and precision. Analysis was conducted for each concentration in three independent extracts. The analytical performance parameters used in the current study are summarized in Table 2. The limit of detection (LOD; 3×SD/m) and quantification (LOQ; 10×SD/m), based on three-times and ten-times of the standard deviation of the blank divided by the slope of the calibration curve with the preconcentration procedure, were 0.15 ng mL^{-1} and 0.5 ng mL^{-1}, respectively. The coefficients of determination (r^2) were also evaluated. According to the results, the linear dynamic range (LR) for the calibration curve with the preconcentration stage was observed in the range of 0.5-40 ng mL^{-1}, with an acceptable correlation coefficient of 0.9994. Meanwhile, LR for the calibration curve without the preconcentration stage was observed in the range of 100-2000 ng mL^{-1}. These results demonstrate the high sensitivity, precision, and reproducibility of the suggested method. The preconcentration factor (PF), a crucial parameter for US-M-A-DMSPE performance, was 60. The enhancement factor (EF), determined as the ratio of the slopes of preconcentrated samples to those obtained without the preconcentration method, was 33.14. This method shows improvements over most of the reported methods and can be considered a qualified method for the preconcentration and determination of Pb (II), serving as an alternative and reliable tool for monitoring trace metals in food matrices. The high selectivity is also a major advantage of the proposed method.

Table 2. Analytical Parameters of Pb (II) determination by of US-M-A-DMSPE-FAAS.

Parameter	Analytical data
Linear dynamic range (ng mL^{-1})	0.5-40
Coefficient of determination	0.9994
Limit of detection (ng mL^{-1})	0.15
Limit of quantification (ng mL^{-1})	0.5
Repeatability (R.S.D., %) (n = 3) ($C_{Pb(II)}$ = 10.0 ng mL^{-1})	2.9
Preconcentration factor (PF)[a]	60
Sample volume (mL)	30

[a] Preconcentration factor is defined as the ratio of sample volume to desorption solvent volume

3.12. Application of the proposed method to water and food samples

The practical applicability of the developed procedure was investigated by determining the concentration of Pb (II) in water, potatoes, carrots, and milk. The accuracy of the proposed procedure was tested by spiking well-known concentrations of Pb (II) and analyzing SRM1570A certified reference material of food samples. The results for these assays are shown in Table 3, demonstrating satisfactory agreement between the achieved results and the certified standards. The relative standard deviations (RSDs) were 2.7-5.6% and 3.6-5.3% for food and water samples, respectively. The recoveries in the range of 85-106% were obtained. These results indicate that the current method has acceptable accuracy and is capable of determining trace of Pb (II) in practical samples with various matrices.

Table 3. The determination of lead in water, potato, carrot and milk samples by the proposed method.

Sample	Added (µg g^{-1})	Found (µg g^{-1})[a]	RSD (%)	Recovery (%)
SRM1570A[b]	-	0.2	3.3	96.5
Potato	-	<LOQ	-	-
	5	0.32	4.4	88
	10	0.64	3.8	91
	15	1.02	4	93
carrot	-	<LOQ	-	-
	5	036	2.7	85
	10	0.82	4.1	101
	15	0.96	4.6	92
milk	0	<LOQ	-	-
	5	0.41	4.6	94
	10	0.86	3.7	99
	15	1.1	5.6	106
Sample	**Added (µg g^{-1})**	**Found (µg g^{-1})[a]**	**RSD (%)**	**Recovery (%)**
Bottled Mineral water	-	<LOQ	-	-
	5	0.34	4.1	97
	10	0.72	4.2	104
	15	0.92	3.6	92
Tap water	-	<LOD	-	-
	5	0.38	4.6	87
	10	0.61	4.4	91
	15	0.98	5.3	90

[a]Mean ± standard deviation (n=3), [b]Certified value: SRM1570A concentration, 0.2 µg g^{-1}

3.13. Comparison with other methods

The analytical performance of the established method for the quantification of Pb (II) was compared with other reported methods (Table 4). It can be observed that the CQD/Fe_3O_4/ZIF-71/PPy sorbent exhibits higher capacity compared to other magnetic sorbents. This novel technique demonstrates higher sensitivity (lower LOD), lower relative standard deviation, or comparable sorbent to other reported methods, along with satisfactory reproducibility. Additionally, the method shows great accuracy and recovery, and the preconcentration time for target metal ions is short. The US-M-A-DMSPE method based on the CQD/Fe_3O_4/ZIF-71/PPy nanocomposite, followed by FAAS, serves as an effective approach for trace monitoring of Pb (II) in water and food samples.

Table 4. The comparison of analytical parameters of the developed US-M-A-DMSPE-FAAS method with other reported methods from some recent studies.

Instrumental technique	Extraction method	Limit of detection (ng mL^{-1})	Relative standard deviation (%)	Sample	PF	Reference
FAAS	MSPE[a]	0.4	3.4	Water, rice, cosmetics	222	[64]
FAAS	SS-MdμSPE –MS[b]	1	3.1	Vegetable, tea, meat, water	80	[65]
FAAS	DMSPE[c]	2.1	5.8	cosmetics	21	[66]
FAAS[d]	RP-UALLME[e]	1.5	1.8	Edible oil		[67]
FAAS	MSPE[f]	0.60	0.87	herbal medicines	33.33	[68]
FAAS	SPE[g]	8.9	5.8	Rice, humber river sediment	20	[69]
FAAS	US-M-A DMSPE	0.15	5.6	water, potato, carrot and milk	60	This work

[a]Magnetic solid-phase extraction (MSPE),[b] Syringe to syringe magnetic dispersive micro solid phase extraction, [c]Dispersive magnetic solid-phase extraction, [d]Flame atomic absorption spectrometry, [e]Reversed-phase ultrasonic assisted liquid−liquid microextraction, [f] Magnetic solid-phase extraction, [g] Solid-phase extraction

4. Conclusion

In this study, an innovative sorbent was synthesized and applied to establish a magnetic solid phase extraction procedure for preconcentration of Pb (II) ions in environmental water and food samples, including carrots, potatoes, milk, mineral water, and tap water, followed by FAAS analysis. The synthesized sorbent was confirmed using FT-IR, SEM, VSM, and XRD techniques. The prepared CQD/Fe_3O_4/ZIF-71/PPy nanocomposite showed several advantages, including high adsorption capacity, excellent reusability, rapid adsorption, and high stability. It significantly improved the analytical characteristics of FAAS compared to several other methods reported in the literature. The advanced method demonstrated sensitivity, accuracy, acceptable repeatability, selectivity, efficient extraction, high preconcentration, and cost-effectiveness. Overall, the results indicate that the new nanocomposite has notable potential in application of selective extraction and preconcentration of Pb (II) ion at trace level in the food samples.

Acknowledgment

The authors would like to gratefully acknowledge the support of this study by Islamic Azad University South Tehran Branch. We are grateful to Ms. Solmaz Karimi and Ms. Hanie Behzad Far for their kindly help in carrying out the FAAS analysis.

References:

[1] A. Sharifi, R. Hallaj, S. Bahar, *J. Anal. Chem*. 1 (2023) 1-10.

[2] E. Yilmaz, I. Ocsoy, N. Ozdemir, M. Soylak, *Anal. Chim. Acta*. 906 (2016) 110-117.

[3] M. Soylak, M. Alasaad, Ö. Özalp, *Microchem. J.* 178 (2022) 107329.

[4] L. Li, B. Hu, L. Xia, Z. Jiang, *Talanta*. 70 (2006) 468-473.

[5] R. C. Machado, A. B. S Silva, C. D. B Amaral, A. Virgilio, A. R. A. Nogueira, *Anal. Methods.* 12 (2020) 39-45.

[6] V. Ivanova-Petropulos, S. Jakabová, D. Nedelkovski, V. Pavlík, Ž. Balážová, O. Hegedűs, *Food Anal. Methods*. 8 (2015) 1947–1952.

[7] R. M. De Oliveira A. C. N, Antunes, M.A. Vieira, A. L. Medina, A. S. Ribeiro, *Microchem. J.* 124 (2016) 402-409.

[8] A. Babaei, M. Zeeb, A. Es-haghi, *J. Sci. Food Agric*. 98 (2018) 3571-3579.

[9] M. Khajeh, S. Pedersen-Bjergaard, M. Bohlooli, A. Barkhordar, M. Ghaffari-Moghaddam Maghemite, *J. Sci. Food Agric*. 97 (2017) 1517-1523.

[10] L. Xu, F. Luan, H. Liu, Y. Gao, *J. Sci. Food Agric.* 95 (2014) 745–751.

[11] M. Salimi, M. Behbahani, H. R. Sobhi, M. Ghambarian, A. Esrafili, *Appl. Organomet. Chem*. 34 (2020) e5715.

[12] N. S. Mdluli, P. N. Nomngongo, N. Mketo, *J. Crit. Rev*. 52 (2022) 1-18.

[13] K. Molaei, H. Bagheri, A. A. Asgharinezhad, H. Ebrahimzadeh, M. Shamsipu, *Talanta*. 15 (2017) 607-616.

[14] R. R. Pasupuleti, Y. L. Huang, *Chin. J. Chem*. 70 (2023) 1326-1337.

[15] M. Mei, J. Pang, X. Huang, Q. Luo, *Anal. Chim. Acta.* 1090 (2019) 82-90.

[16] S. Khodadadi, E. Konoz, A. Niazi, A. Ezabadi, *Chemical Papers.* 76 (2022) 6735–6751.

[17] L. Suo, X. Dong, X. Gao, J. Xu, Z. Huang, J. Ye, X. Lu, L. Zhao, *Microchem. J*. 149 (2019) 104039.

[18] E. Bozorgzadeh, A. Pasdaran, H. Ebrahimi-Najafabadi, *Food Chem*. 346 (2020) 128916.

[19] E. Ziaei, A. Mehdinia, A. Jabbari, *Anal. Chim. Acta*. 850 (2014) 49-56.

[20] M. Mashkani, A. Mehdinia, A. Jabbari, Y. Bide, M. R. Nabid, *Food Chem.* 239 (2018) 1019-1026.

[21] Y. Liu, J. Hu, Y. Li, H. P. Wei, X. S. Li, X. H. Zhang, S. M. Chen, X. Q. Chen, *Talanta*. 134 (2017) 16-23.

[22] Á. Santana-Mayor, R. Rodríguez-Ramos, B. S. Rodríguez, M. Asensio-Ramos, M. Á. *Sep. Sci.* (2020) 83-127.

[23] E. Yilmaz, M. Soylak, *J. Nanomater*. (2020) 375-413.

[24] Z. Najafi, S. Esmaili, B. Khaleseh, S. Babaee, M. Khoshneviszadeh, G. Chehardoli, T. Akbarzadeh, *Sci. Rep*. 12 (2022) 19917.

[25] H. Asadollahzadeh, M. Ghazizadeh, M. Manzari, *Environ. Sci. Nano.* 4 (2021) 33-46.

[26] H. M. Pérez-Cejuela, J. M. Herrero-Martínez, E. F. Simó-Alfonso, *Mol*. 25 (2020) 4216.

[27] W. Ma, X. Li, Y. Bai, H. Liu, *Trends Anal. Chem*. 109 (2018) 154-162.

[28] H. M. Pérez-Cejuela, F. Benavente, E. F. Simó-Alfonso, J. M. Herrero-Martínez. *Talanta*. 233 (2021) 122529.

[29] L. Hao, X. Liu, J. Wang, C. Wang, Q. Wu, Z. Wang, *Talanta*. 142 (2015) 104-109.

[30] Q. Zhou, L. Zhu, X. Xia, H. Tang, *Microchim Acta*. 183 (2016) 1839–1846.

[31] Y. Sanaei, M. Zeeb, S. S. Homami, A. Monzavi, Z. Khodadadi, *RSC Adv*. 11 (2021) 30361-30372.

[32] X. Dong, Y. S. Lin, Synthesis of an organophilic ZIF-71 membrane for pervaporation solvent separation. *Chem. Commun*. 49 (2013) 1196-1198.

[33] Y. Sanaei, M. Zeeb, S. S. Homami, A. Monzavi, Z. Khodadadi, *Anal. Chem*. 5 (2022) 60-75.

[34] T. Zhou, Y. Sang, Y. Sun, C. Wu, *Langmuir*. 35 (2019) 3248–3255.

[35] Y. Zhou, T. Zhou, Y. Zhang, L. Tang, Q. Guo, *Solid State Ion*. 350 (2020) 115278.

[36] J. Duan, D. Shao, X. He, Y. Lu, W. Wang, Colloids Surf. A: Physicochem. *Eng. Asp*. 619 (2021) 126529.

[37] A. M. Devasurendra, D. S. W. Palagama, A. Rohanifar, D. Isailovic, J. R. Kirchhoff, J. L. Anderson, *J. Chromatogr*. A. 1560 (2018) 1-9.

[38] A. Amiri, M. Baghayeri, M. Shahabizadeh, *New J Chem*. 47 (2023) 4402-4408.

[39] F. Qi, X. Li, B. Yang, F. Rong, Q. Xu, *Talanta*. 144 (2015) 129-135.

[40] X. Lai, C. Liu, H. He, J. Li, L. Wang, Q. Long, P. Zhang, Y. *Ferroelectrics*. 566 (2020) 116-123.

[41] R. P. Lively, M. E. Dose, J. A. Thompson, A. M. Benjamin, R. R. Chance, W. J. Koros, *Chem. Commun*. 47 (2011) 8667–8669.

[42] S. Japip, H. Wang, Y. Xiao, T. S. Chung, *J. Membr. Sci*. 467 (2014) 162–74.

[43] E. Nakhostin Mortazavi, M. Zeeb, S. S. Homami, *Anal. Lett*. 57 (2023) 425-444.

[44] Z. Najafi, S. Esmaili, B. Khaleseh, S. Babaee, M. Khoshneviszadeh, G. Chehardoli, T. Akbarzadeh, *Sci. Rep.* 12 (2022) 19917.

[45] B. Chen, Z. Yang, Y. Zhu, Y. Xia, *J. Mater. Chem. A.* 2 (2014) 16811-16831.

[46] S. Farid, W. Qiu, J. Zhao, X. Song, Q. Mao, S. Ren, C. Hao, *J. Electroanal. Chem*. 858 (2020) 113768.

[47] S. Sagar Mittal, G. Ramadas, N. Vasanthmurali, V. S. Madaneshwar, M. Sathish Kumar, N. K. Kothurkar, *Mater. Sci. Eng.* 577 (2019) 012194.

[48] P. S. Saud, B. Pant, M. Park, Z. K. Ghouri, H. Y. Kim, A. M. Alam, *Ceram. Int*. 41 (2015) 11953-11959.

[49] H. Eskalena, S. Uruş, Ş. Özgang, S. Bahattin, *Ind. Crops. Prod*. 147 (2020) 112209.

[50] S. Sajjadi, A. Khataee, R. Darvishi Cheshmeh Soltani, A. N. Hasanzadeh, *J. Phys. Chem. Solids*. 127 (2018) 140-150.

[51] B. Habibi, S. Pashazadeh, L.A. Saghatforoush, A. Pashazadeh, *New J Chem*. 45 (2021) 14739-14750.

[52] Y. Chen, W. Huang, K. Chen, T. Zhang, Y. Wang, J. Wang, *Sens. Actuators. B. Chem.* 290 (2018) 434-442.

[53] S. Farid, W. Qiu, J. Zhao, X. Song, Q. Mao, S. Ren, C. Hao, *J. Electroanal. Chem.* 2019; 858: 113768.

[54] S. Abolghasemzade, M. Pourmadadi, H. Rashedi, F. Yazdian, S. Kianbakht, M. Navaei-Nigjeh, *J. Mater. Chem. B.* 9 (2021) 658-676.

[55] T. Akbarpour, A. Khazaei, J. Yousefi Seyf, N. Sarmasti, *Appl. Organomet. Chem*. 35 (2021) e6361.

[56] X. Wei, Y. Wang, Y. Huang, C. Fan, *J. Alloys Compd*. 802 (2019) 467-476.

[57] X. Jian, J. G. Li, H. M. Yang, L. I. Cao, E. H. Zhang, Z. H. Liang, *Carbon*. 114 (2017) 533-543.

[58] Y. Bi, M. Ma, Y. Liu, Z. Tong, R. Wang, K. Chung, A. Ma, G. Wu, Y. Ma, C. He, P. Liu, L. Hu, *J. Colloid Interface Sci*. 600 (2021) 209-218.

[59] C. Hou, D. Zhao, Y. Wang, S. Zhang, S. Li, *J. Electroanal. Chem*. 822 (2017) 50-56.

[60] M. Yahya, S. Kesekler, I. Durukan, Ç. Arpa, *Anal. Methods.* 13 (2021) 1058-1068.

[61] D. Fitriana, M. Mudasir, D. Siswanta, *Key Eng. Mater*. 840 (2019) 57-63.

[62] X. Zhao, L. Baharinikoo, Davoodabadi M. Farahani, B. Mahdizadeh, A. A. Kazemzadeh Farizhandi, *Sci. Rep*. 12 (2022) 5987.

[63] H. R. Sobhi, A. Mohammadzadeh, M. Behbahani, A. Esrafili, *Microchem. J.* 146 (2019) 146: 782-788.

[64] Z. Mehrani, Z. Karimpour, H. Ebrahimzadeh, *New J Chem*. 44 (2020) 15000-15009.

[65] S. Arghavani-Beydokhti, M. Rajabi, A. Asghari, *Anal. Methods*. 10 (2018) 1305-1314.

[66] M. Rajabi, Z. Mollakazemi, M. Hemmati, S. Arghavani-Beydokhti, *Anal. Methods*. 12 (2020) 4867–4877.

[67] M. Mohebbi, R. Heydari, M. Ramezani, *J. Anal. Chem*. 73 (2018) 73: 30–35.

[68] P. Jamshidi, F. Shemirani, *Microchim. Acta*. 185 (2018) 421.

[69] M. Soylak, E. Yilmaz, M. Ghaedi, M. Montazerozohori, *Toxicol. Environ. Chem*. 93 (2012) 873-885.